Efficient Multicarrier Communication for Highly Spread Underwater Acoustic Channels

Sung-Jun Hwang and Philip Schniter

Abstract—In this paper we propose a novel method for communication over underwater acoustic channels that exhibit simultaneously large delay spread and Doppler spread, such as those found in the surf zone. In particular, we propose a coded pulse-shaped multicarrier scheme that converts the doubly dispersive channel into an inter-carrier interference (ICI) channel with small ICI spread. The resulting ICI is mitigated using a soft noncoherent equalizer that leverages sparsity in the delay-power profile to generate near-optimal bit estimates with low complexity. The noncoherent equalizer uses a delay-power-profile estimate (rather than a channel estimate) which is obtained from pilots. Numerical simulations with surf-zone-like channels demonstrate performance close to genie-aided bounds.

Index Terms—Underwater acoustic modems, underwater acoustic channels, multicarrier modulation, noncoherent decoding, turbo equalization, joint estimation and detection, sparse channels.

I. INTRODUCTION

THE UNDERWATER acoustic channel (UAC) has been referred to as "quite possibly nature's more unforgiving wireless medium" [1]. The physical characteristics of the UAC are highly dependent on the distance and relative movement between the transmitter and receiver; the proximity, roughness, and motion of the scattering surfaces; and the presence of ambient interference. However, the factors that pose the primary challenges for data communication over the UAC can be summarized as *simultaneously large delay- and Doppler-spreads*, *limited bandwidth*, and *limited receiver complexity*. These challenges can be understood as follows. Large delay-spread implies that single-carrier communication will be plagued by inter-symbol interference (ISI) that, for practical signal bandwidths, spans hundreds of symbols. Large Doppler-spread then implies that this ISI response will change quickly in time. Since optimal mitigation of this long and quickly-varying ISI response becomes computationally infeasible, practitioners have resorted to simple sub-optimal strategies such as the adaptive decision-feedback equalization (DFE) [2], [3]. However, these implementable single-carrier

techniques perform far short of optimal and fail altogether in very highly spread environments such as the surf zone [4].

As an alternative, multi-carrier modulation (MCM) has been proposed to increase the symbol interval and thereby decrease the ISI span. While a number of MCM proposals for the UAC have been made over the years (see, e.g., the recent work [5]–[7]), none seem to have been successful enough to displace single-carrier/DFE as the practical method of choice. The primary difficulty in applying MCM to the doubly dispersive UAC is that, as the symbol interval is increased (to reduce ISI span), the subcarrier spacing must be decreased (to preserve data rate and transmission bandwidth), making the system more susceptible to Doppler-spread-induced inter-carrier interference (ICI). Thus, barring a decrease in spectral efficiency, ISI reduction comes at the expense of ICI escalation.

A close look at recent MCM proposals helps to illuminate the challenges in applying MCM to the surf zone UAC. The works [5] and [6], for example, proposed classical ZP-OFDM signaling schemes assuming that the Doppler-spread was small enough to induce *negligible* ICI. For these schemes, the universal ICI bound[1] in [8] implies that an ICI power of -25 dB (which we consider to be "negligible") occurs when $f_D T_s = 0.03$, where f_D denotes the single-sided Doppler-spread and T_s the MCM-symbol duration. Since T_s was chosen as $7T_h$ (as $3.4T_h$) in [5] (in [6]), where T_h denotes delay-spread, we deduce that these schemes can handle UACs with a delay/Doppler-spread product of at most $f_D T_h = 0.004$ ($f_D T_h = 0.009$). The surf-zone channels[2] described in [4], however, yield $f_D T_h \approx 0.1$, which is $25\times$ ($10\times$) as severe. As another example, in the non-traditional MCM approach [7], the symbol length was chosen shorter than that needed for perfect ISI-suppression, in order to tolerate high Doppler-spread while keeping ICI negligible. The resulting ISI-span was short enough to enable the use of sophisticated joint estimation/detection techniques (i.e., LMS/Viterbi per-survivor processing [9]), which were shown to significantly outperform the traditional adaptive DFE. But [7] only demonstrated the ability to handle $f_D T_h = 0.0035$ via simulation and $f_D T_h \approx 0.002$ experimentally, which are over 30 times milder than the surf-zone channels discussed in [4]. Finally, the recent work [10] makes the ZP-OFDM negligible-ICI assumption after compensating for Doppler frequency *shift* due to a moving platform. However, their scheme failed when the transmitter passed by the receiver, i.e., when the Doppler frequency shift *changed* from positive to negative. There, the platform motion caused a Doppler frequency *spread*. Thus, the literature

The authors are with the Department of Electrical and Computer Engineering at The Ohio State University, Columbus, OH 43210. (e-mail: schniter@ece.osu.edu; hwangsu@ece.osu.edu).

---

[1]The analysis in [8] confirms that this bound is tight for $f_D T_s = 0.03$.
[2]For these channels it was found that $f_D \approx 15$ Hz and $T_h \approx 7$ ms.

appears to fall short of an MCM scheme that is suitable for communication over highly spread surf-zone UACs.

The general problem of communicating over doubly dispersive channels, i.e., those with simultaneously large delay and Doppler spreads, has received significant attention from theoreticians over the last two decades. Most of them have approached this problem through the design of MCM pulse-shapes which minimize total ISI/ICI power (e.g., [11]–[14]), with the goal of making ISI/ICI negligible. But, even with optimized pulses, ISI/ICI remains[3] non-negligible for channels whose delay/Doppler product $f_D T_h$ is commensurate with that of the surf-zone—a fundamental consequence of the Balian-Low theorem from Gabor theory [13]. This fact led the authors to propose a non-traditional approach in which a small ICI span (e.g., 1 or 2 subcarriers) is tolerated and MCM pulse shapes are designed to minimize *residual* ISI/ICI power [15]. In this case, near-perfect residual-ISI/ICI suppression can be accomplished *without* loss of spectral efficiency, and high-performance dominant-ICI mitigation can be accomplished with low complexity. In this paper, we discuss how such an approach can be applied for communication over the UAC.

The aforementioned ISI/ICI mitigation schemes require (implicitly or explicitly) accurate channel state information (CSI). Maintaining this CSI is especially difficult when the channel is doubly dispersive, due to the typically large number of channel coefficients and their fast rate-of-change. Pilot-aided transmission (PAT) [16] is a practical means of aiding data reception in the presence of channel uncertainty. PAT is often used with *decoupled* channel-estimation/data-decoding, where a channel estimate is first obtained via pilots and later used for coherent data decoding. To minimize the MMSE of pilot channel estimates, it is necessary to keep the channel estimates free of interference from unknown data [17] (especially at high SNR), though doing so with a doubly dispersive channel requires time/frequency guards have been shown to sacrifice achievable spectral efficiency [18]. When PAT is used with *joint* estimation/decoding (JED), however, there is no need to separate pilots and data, allowing spectrally efficient communication over the doubly dispersive channel [18]. These facts motivate the consideration of PAT with JED for the UAC.

As one would expect, the complexity of optimal JED is prohibitive. Practical JED requires the use of simplified channel models and approximations of the optimal maximum *a posteriori* (MAP) decoding metric. For example, it is common to model the channel as first-order Gauss-Markov and to apply trellis-based decoding methods with either forward-backward or fixed-lag MAP processing [19]. Still, this framework does not appear practical for highly dispersive channels like the UAC, whose impulse response spans hundreds of symbols and changes quickly. With this in mind, the authors proposed a novel noncoherent equalizer [20] which uses soft tree-search and leverages a basis-expansion model (BEM) [21] for the time-varying channel. The result is near-MAP performance with a per-symbol complexity that scales as only $\mathcal{O}(N_h^2 D^2)$, where $N_h = T_h/T_c$ denotes the delay-spread (in chips)

and $D = \lceil f_D T_c N \rceil$ the single-sided Doppler spread (in subcarriers). Here, T_c denotes the "chip" interval, i.e., the inverse signal bandwidth. With surf-zone UAC parameters, however, the complexity remains prohibitive. For example, if 7.5 kHz bandwidth was used to communicate over the surf-zone UAC in [4], one can expect $N_h \approx 50$, for which the N_h^2 dependence may be problematic.

The key to the complexity puzzle may lie in the sparse nature of realistic UAC responses [22], [23]. For example, if only $1/3$ of the channel's N_h delay taps are significant, then a reception algorithm whose complexity is quadratic in the *active* delay taps (versus total delay taps) will save by a factor of 9. But designing a receiver capable of leveraging sparsity in this manner is non-trivial, especially for MCM schemes like [5]–[7]. In fact, most sparsity-leveraging algorithms are based on adaptive DFE (e.g., [23]), whose performance is known to fall far short of optimal. Another challenge to leveraging sparsity is accurate tracking of the locations of active taps, which can change quite rapidly (see, e.g., [4]). While clever order-recursive matching-pursuit algorithms have been proposed for this purpose (e.g., [23]), their complexity remains quadratic in the full channel length N_h, which (as we have seen) can be very large; we want something simpler.

In this paper, we propose a turbo JED receiver, building on our earlier work [20], [24], that operates in a pulse-shaped MCM framework and which takes full advantage of sparsity in the channel delay profile. Our approach uses a sparse Fourier BEM to model frequency-domain channel variation and a fast tree-search to compute the soft noncoherent equalizer outputs. In addition, we propose a simple pilot-aided means of tracking the channel's quickly-varying delay-power profile. The performance of our algorithm is evaluated numerically using simulated channels whose sparsity and delay/Doppler spreads mimic those of the surf-zone channels from [4]. The proposed scheme is found to exhibit excellent BER performance relative to genie-aided bounds, while maintaining high spectral efficiency and relatively low complexity.

Notation: We use $(\cdot)^T$ to denote transpose, $(\cdot)^*$ conjugate, and $(\cdot)^H$ conjugate transpose, and we use $[\boldsymbol{B}]_{m,n}$ to denote the element in the mth row and n^{th} column of matrix $\boldsymbol{B}$, where row/column indices begin with zero. We also use $\mathcal{D}(\boldsymbol{b})$ to denote the diagonal matrix created from vector $\boldsymbol{b}$, $\boldsymbol{I}_K$ the $K \times K$ identity matrix, and $\{\delta_k\}$ the Kronecker delta sequence. Finally, we use $\odot$ to denote element-wise multiplication, $\langle\cdot\rangle_N$ modulo-N operation, and $\mathrm{E}\{\cdot\}$ expectation.

II. SYSTEM MODEL

First we describe a discrete-time complex-baseband model of our system, which includes coded multicarrier modulation (MCM) and a sparse doubly dispersive channel.

A. Pulse-Shaped MCM

At the transmitter, information bits are rate-R coded and mapped to 2^Q-ary scalar data symbols. Groups of N_s scalar data symbols are then combined with scalar pilot/guard symbols to form transmission blocks of length $N \geq N_s$. (Pilot and guard details will be given later.) Using N subcarriers, the ith MCM-symbol is composed of the scalar symbols

---

[3]The ISI/ICI power is significant unless the MCM subcarrier/symbol spacing is increased to about twice the Nyquist spacing, thereby incurring a significant decrease in spectral efficiency which would be very undesirable for the bandwidth-limited UAC.

$\{c_k^{(i)}\}_{k=0}^{N-1}$ corresponding to the coded bits $\{x_j^{(i)}\}_{j=0}^{N_sQ-1}$. In particular, the jth scalar symbol is mapped from the coded bits $\underline{\boldsymbol{x}}_j^{(i)} := [x_{jQ}^{(i)}, \ldots, x_{jQ+Q-1}^{(i)}]^T$. The transmitted sequence $\{t_n\}$ is generated by transforming the ith MCM-symbol sequence $\{c_k^{(i)}\}_{k=0}^{N-1}$ with an N-point inverse discrete Fourier transform (DFT), applying an N_α-point modulation pulse $\{\alpha_n\}_{n=0}^{N_\alpha-1}$ to its cyclic extension, and superimposing the result N samples behind the contribution from the $(i-1)^{th}$ MCM-symbol:

$$t_n = \sum_{i=-\infty}^{\infty} \alpha_{n-iN} \frac{1}{\sqrt{N}} \sum_{k=0}^{N-1} c_k^{(i)} e^{j\frac{2\pi}{N}kn}. \qquad (1)$$

(See [15] for a slightly more general scheme.) A noisy linear time-varying channel then produces the received samples

$$r_n = \sum_{l=0}^{N_h-1} h_{n,l} t_{n-l} + v_n, \qquad (2)$$

where $\{h_{n,l}\}_{l=0}^{N_h-1}$ denotes the length-N_h discrete impulse response at time n, and where $\{v_n\}$ is zero-mean circular white Gaussian noise (CWGN) with variance σ^2. In relation to the ith MCM-symbol, we define $r_n^{(i)} := r_{iN+n}$, $v_n^{(i)} := v_{iN+n}$, and $h_{n,l}^{(i)} := h_{iN+n,l}$ and rewrite (2) as (3). For demodulation, the receiver applies the length-N_β pulse $\{\beta_n\}_{n=0}^{N_\beta-1}$ prior to an N-point DFT, yielding the frequency-domain observations $\{y_d^{(i)}\}_{d=0}^{N-1}$:

$$y_d^{(i)} = \frac{1}{\sqrt{N}} \sum_{n=0}^{N_\beta-1} r_n^{(i)} \beta_n e^{-j\frac{2\pi}{N}dn}. \qquad (4)$$

Putting (1)-(4) together, it is straightforward to show that

$$y_d^{(i)} = \sum_{\ell=-\infty}^{\infty} \sum_{k=0}^{N-1} H_{d-k,k}^{(i,\ell)} c_k^{(i-\ell)} + w_d^{(i)}, \qquad (5)$$

$$H_{d,k}^{(i,\ell)} := \frac{1}{N} \sum_{n=0}^{N_\beta-1} \sum_{l=0}^{N_h-1} h_{n,l}^{(i)} \beta_n \alpha_{\ell N+n-l} e^{-j\frac{2\pi}{N}(dn+kl)} \qquad (6)$$

$$w_d^{(i)} := \frac{1}{\sqrt{N}} \sum_{n=0}^{N_\beta-1} \beta_n v_n^{(i)} e^{-j\frac{2\pi}{N}dn}. \qquad (7)$$

In writing (5), we used the fact that $H_{d,k}^{(i,\ell)}$ is N-cyclic in the indices d and k. Note that $H_{d,k}^{(i,\ell)}$ can be interpreted as the response, at MCM-symbol i and subcarrier $k+d$, to a frequency-domain impulse applied at MCM-symbol $i-\ell$ and subcarrier k. Using $\boldsymbol{y}^{(i)} := [y_0^{(i)}, \ldots, y_{N-1}^{(i)}]^T$, $\boldsymbol{c}^{(i)} := [c_0^{(i)}, \ldots, c_{N-1}^{(i)}]^T$, and $\boldsymbol{w}^{(i)} := [w_0^{(i)}, \ldots, w_{N-1}^{(i)}]^T$, (5) can be written in vector form as

$$\boldsymbol{y}^{(i)} = \sum_{\ell=-\infty}^{\infty} \sum_{k=0}^{N-1} \mathcal{D}_k(\boldsymbol{c}^{(i-\ell)}) \boldsymbol{H}_{-k}^{(i,\ell)} + \boldsymbol{w}^{(i)} \qquad (8)$$

$$\boldsymbol{H}_d^{(i,\ell)} := [H_{d,-d}^{(i,\ell)}, H_{d,-d+1}^{(i,\ell)}, \ldots, H_{d,N-1-d}^{(i,\ell)}]^T \in \mathbb{C}^N, \qquad (9)$$

where $\mathcal{D}_k(\cdot)$ denotes the diagonal matrix created from the k-place cyclic downward shift of its vector argument, i.e., $[\mathcal{D}_k(\boldsymbol{c})]_{d,d} = c_{\langle d-k \rangle_N}$.

Although from (1) it can be seen that no time-domain guard is employed by the transmitter, it is possible (see, e.g., [15]) to design pulses $\{\alpha_n\}$ and $\{\beta_n\}$ that yield both negligible

ISI (i.e., $H_{d,k}^{(i,\ell)} \approx 0$ for $\ell \neq 0$) and negligible ICI beyond a radius of $D := \lceil f_D T_c N \rceil$ subcarriers (i.e., $H_{d,k}^{(i,\ell)} \approx 0$ for $D < d < N - D$). With zero ISI and an ICI radius of D, (8) becomes

$$\boldsymbol{y}^{(i)} = \sum_{k=-D}^{D} \mathcal{D}_k(\boldsymbol{c}^{(i)}) \boldsymbol{H}_{-k}^{(i,0)} + \boldsymbol{w}^{(i)}. \qquad (10)$$

B. A Sparsity Leveraging Frequency-Domain BEM

We now develop a sparse basis expansion model (BEM) for the frequency-domain channel coefficient vector $\boldsymbol{H}_d^{(i,0)}$. From (6) and (9) it can be seen that

$$\boldsymbol{H}_d^{(i,0)} = \boldsymbol{F} \breve{\boldsymbol{\theta}}_d^{(i)} \qquad (11)$$

$$\breve{\boldsymbol{\theta}}_d^{(i)} := \sqrt{N} \mathcal{D}(\boldsymbol{f}_d^*)(\mathcal{H}^{(i)} \odot \mathcal{P})^T \underline{\boldsymbol{f}}_d \in \mathbb{C}^N, \qquad (12)$$

where $\mathcal{H}^{(i)}, \mathcal{P} \in \mathbb{C}^{N_\beta \times N}$ are defined element-wise as $[\mathcal{H}^{(i)}]_{n,l} := h_{n,l}^{(i)}$ and $[\mathcal{P}]_{n,l} := \beta_n \alpha_{n-l}$, where $\boldsymbol{F}$ denotes the unitary N-DFT matrix (i.e., $[\boldsymbol{F}]_{n,m} = \frac{1}{\sqrt{N}} e^{-j\frac{2\pi}{N}nm}$) with d^{th} column $\boldsymbol{f}_d \in \mathbb{C}^N$, and where $\underline{\boldsymbol{f}}_d := [e^{-j\frac{2\pi}{N}d\cdot 0}, e^{-j\frac{2\pi}{N}d\cdot 1}, \ldots, e^{-j\frac{2\pi}{N}d(N_\beta-1)}]^T$ denotes the latter's N_β-length (cyclic) extension. Equation (11) can be recognized as an Nth-order BEM for the frequency-domain channel vector $\boldsymbol{H}_d^{(i,0)}$; the columns of $\boldsymbol{F}$ are the basis vectors and elements of $\breve{\boldsymbol{\theta}}_d^{(i)}$ are the BEM coefficients.

The BEM order can be reduced if the impulse response is known to be sparse. In particular, if only $N_a < N_h$ taps of the impulse response $\{h_{n,l}^{(i)}\}_{l=0}^{N_h-1}$ are non-zero over the time duration $n \in \{0, \ldots, N_\beta - 1\}$, then only N_a columns of $\mathcal{H}^{(i)}$ will be non-zero, implying that only N_a BEM coefficients in $\breve{\boldsymbol{\theta}}_d^{(i)}$ will be non-zero. More precisely, let us denote the set of channel taps active during the ith MCM-symbol interval by

$$\mathcal{L}^{(i)} = \{l : h_{n,l}^{(i)} \neq 0 \text{ for some } n \in \{0, \ldots, N_\beta - 1\}\}(13)$$

where $|\mathcal{L}^{(i)}| = N_a$. Constructing $\boldsymbol{B}^{(i)} \in \mathbb{C}^{N \times N_a}$ from the columns of $\boldsymbol{F}$ with indices in $\mathcal{L}^{(i)}$, and constructing $\boldsymbol{\theta}_d^{(i)} \in \mathbb{C}^{N_a}$ from the corresponding elements of $\breve{\boldsymbol{\theta}}_d^{(i)}$, (11) can be restated as

$$\boldsymbol{H}_d^{(i,0)} = \boldsymbol{B}^{(i)} \boldsymbol{\theta}_d^{(i)}. \qquad (14)$$

Using this "compressed" BEM, (10) can be rewritten as (15) and (16).

Notice that the BEM $\boldsymbol{B}^{(i)}$ changes with the MCM-symbol index.

C. Modifications for Noncoherent Soft Equalization

In Section III-B, we describe a noncoherent soft equalization scheme based on tree search. A frequency-domain guard pattern that facilitates this tree search will now be described.

From (15), it can be seen that every element in $\boldsymbol{y}^{(i)}$ sees contributions from $2D + 1$ subcarriers. For tree search, we would like that the first observation contains a contribution from only one unknown scalar symbol, the second contains contributions from only two unknown scalar symbols, the third from only three unknown scalar symbols, and so on. One way to ensure this is to set $\{c_{\langle k \rangle_N}^{(i)}\}_{k=-D}^{D-1} = 0$, i.e., to "turn off" the

$$r_n^{(i)} = \sum_{l=0}^{N_h-1} h_{n,l}^{(i)} \sum_{\ell=-\infty}^{\infty} \alpha_{\ell N+n-l} \sum_{k=0}^{N-1} c_k^{(i-\ell)} \frac{e^{j\frac{2\pi}{N}k(n-l)}}{\sqrt{N}} + v_n^{(i)}. \tag{3}$$

$$\boldsymbol{y}^{(i)} = \left[\mathcal{D}_D(\boldsymbol{c}^{(i)})\boldsymbol{B}^{(i)}, \ldots, \mathcal{D}_{-D}(\boldsymbol{c}^{(i)})\boldsymbol{B}^{(i)} \right] \boldsymbol{\theta}^{(i)} + \boldsymbol{w}^{(i)} \tag{15}$$

$$\boldsymbol{\theta}^{(i)} := [\boldsymbol{\theta}_{-D}^{(i)T}, \ldots, \boldsymbol{\theta}_D^{(i)T}]^T \tag{16}$$

first and last D subcarriers—a technique commonly used to prevent adjacent-channel interference in channelized systems. Note that the resulting loss in spectral efficiency will be small when $2D \ll N$.

To proceed further, it is convenient to define the D-shifted quantities $\bar{c}_k^{(i)} = c_{\langle k+D\rangle_N}^{(i)}$ and $\bar{\boldsymbol{c}}^{(i)} := [\bar{c}_0^{(i)}, \ldots, \bar{c}_{N-1}^{(i)}]^T$, noticing that the last $2D$ elements in $\bar{\boldsymbol{c}}^{(i)}$ constitute a zero-valued guard interval. Since $\mathcal{D}_k(\bar{\boldsymbol{c}}^{(i)}) = \mathcal{D}_{k-D}(\boldsymbol{c}^{(i)})$ for any k, we can rewrite (15) as

$$\boldsymbol{y}^{(i)} = \boldsymbol{A}^{(i)}\boldsymbol{\theta}^{(i)} + \boldsymbol{w}^{(i)} \tag{17}$$

$$\boldsymbol{A}^{(i)} := \left[\mathcal{D}_{2D}(\bar{\boldsymbol{c}}^{(i)})\boldsymbol{B}^{(i)}, \ldots, \mathcal{D}_0(\bar{\boldsymbol{c}}^{(i)})\boldsymbol{B}^{(i)} \right] \tag{18}$$

and see that, for each $k \in \{0, \ldots, N-1\}$, the observations $\{y_d^{(i)}\}_{d=0}^k$ depend only on $\{\bar{c}_d^{(i)}\}_{d=0}^k$. The now "causal" ICI channel allows us to write the partial observation $\boldsymbol{y}_k^{(i)} := [y_0^{(i)}, \ldots, y_k^{(i)}]^T$ as

$$\boldsymbol{y}_k^{(i)} = \boldsymbol{A}_k^{(i)}\boldsymbol{\theta}^{(i)} + \boldsymbol{w}_k^{(i)}, \tag{19}$$

where $\boldsymbol{w}_k^{(i)} := [w_0^{(i)}, \ldots w_k^{(i)}]^T$ and where $\boldsymbol{A}_k^{(i)}$ appends a new row $\boldsymbol{a}_k^{(i)H} \in \mathbb{C}^{(2D+1)N_a}$ with each k:

$$\boldsymbol{A}_k^{(i)} = \begin{bmatrix} \boldsymbol{a}_0^{(i)H} \\ \vdots \\ \boldsymbol{a}_k^{(i)H} \end{bmatrix} \tag{20}$$

$$\boldsymbol{a}_k^{(i)H} = [\bar{c}_{k-2D}^{(i)}\boldsymbol{b}_k^{(i)H}, \ldots, \bar{c}_k^{(i)}\boldsymbol{b}_k^{(i)H}]. \tag{21}$$

In (21), $\boldsymbol{b}_k^{(i)H}$ denotes the kth row of $\boldsymbol{B}^{(i)}$. Note that the full-block quantities $\boldsymbol{y}_{N-1}^{(i)}$, $\boldsymbol{A}_{N-1}^{(i)}$, $\bar{\boldsymbol{c}}_{N-1}^{(i)}$, and $\boldsymbol{w}_{N-1}^{(i)}$ are identical to the previously defined $\boldsymbol{y}^{(i)}$, $\boldsymbol{A}^{(i)}$, $\bar{\boldsymbol{c}}^{(i)}$, and $\boldsymbol{w}^{(i)}$, respectively.

Finally, we investigate the cross-covariance matrix $\boldsymbol{R}_{\boldsymbol{\theta}_d,\boldsymbol{\theta}_k}^{(i)} := \mathrm{E}\{\boldsymbol{\theta}_d^{(i)}\boldsymbol{\theta}_k^{(i)H}\}$ for later use in tree-search. We assume that the channel obeys the wide-sense stationary uncorrelated scattering (WSSUS) assumption over the duration of one MCM-symbol, i.e.,

$$\mathrm{E}\{h_{n,l}^{(i)}h_{n-m,l'}^{(i)*}\} = \rho_m^{(i)}\sigma_l^{(i)2}\delta_{l-l'} \text{ for } 0 \le n < N_\beta, \tag{22}$$

where $\{\sigma_l^{(i)2}\}_{l=0}^{N_h-1}$ is the delay-power profile (DPP) and $\{\rho_m^{(i)}\}$ is the normalized (i.e., $\rho_0^{(i)} = 1$) tap autocorrelation sequence during the ith MCM-symbol interval. Furthermore, we assume that $\{\rho_m^{(i)}\}$ is invariant to i and thus suppress the superscript notation.

Using the definition of $\breve{\boldsymbol{\theta}}_d^{(i)}$ in (12) and the fact that $\boldsymbol{\theta}_d^{(i)}$ is constructed from the N_a active taps in $\breve{\boldsymbol{\theta}}_d^{(i)}$, the νth element of $\boldsymbol{\theta}_d^{(i)}$ can be written as

$$\left[\boldsymbol{\theta}_d^{(i)}\right]_\nu = \frac{1}{\sqrt{N}} \sum_{n=0}^{N_\beta-1} \beta_n \alpha_{n-l_\nu^{(i)}} h_{n,l_\nu^{(i)}}^{(i)} e^{-j\frac{2\pi}{N}d(n-l_\nu^{(i)})} \tag{23}$$

where $l_\nu^{(i)}$ denotes the index of the νth active tap (i.e., $\mathcal{L}^{(i)} = \{l_0^{(i)}, l_1^{(i)}, \ldots, l_{N_a-1}^{(i)}\}$). The $(\nu, \nu')^{th}$ element of the cross-covariance matrix $\boldsymbol{R}_{\boldsymbol{\theta}_d,\boldsymbol{\theta}_k}^{(i)}$ can then be written as

$$\left[\boldsymbol{R}_{\boldsymbol{\theta}_d,\boldsymbol{\theta}_k}^{(i)}\right]_{\nu,\nu'} = \frac{1}{N}\mathrm{E}\left\{ \sum_{p=0}^{N_\beta-1} \beta_p \alpha_{p-l_\nu^{(i)}} h_{p,l_\nu^{(i)}}^{(i)} e^{-j\frac{2\pi}{N}d(p-l_\nu^{(i)})} \right.$$
$$\left. \times \sum_{q=0}^{N_\beta-1} \beta_q^* \alpha_{q-l_{\nu'}^{(i)}}^* h_{q,l_{\nu'}^{(i)}}^{(i)*} e^{j\frac{2\pi}{N}d(q-l_{\nu'}^{(i)})} \right\} \tag{24}$$

The WSSUS assumption (22) specifies that $\mathrm{E}\{h_{p,l_\nu^{(i)}}^{(i)}h_{q,l_{\nu'}^{(i)}}^{(i)*}\} = 0$ when $\nu' \ne \nu$, implying that $\boldsymbol{R}_{\boldsymbol{\theta}_d,\boldsymbol{\theta}_k}^{(i)}$ is diagonal. Furthermore, since $\mathrm{E}\{h_{p,l_\nu^{(i)}}^{(i)}h_{q,l_\nu^{(i)}}^{(i)*}\} = \sigma_{l_\nu^{(i)}}^{(i)2}\rho_{p-q}$, we find

$$\left[\boldsymbol{R}_{\boldsymbol{\theta}_d,\boldsymbol{\theta}_k}^{(i)}\right]_{\nu,\nu} = \sigma_{l_\nu^{(i)}}^{(i)2}\frac{1}{N}\sum_{p=0}^{N_\beta-1} \beta_p \alpha_{p-l_\nu^{(i)}} e^{-j\frac{2\pi}{N}d(p-l_\nu^{(i)})}$$
$$\times \sum_{q=0}^{N_\beta-1} \rho_{p-q}\beta_q^* \alpha_{q-l_\nu^{(i)}}^* e^{j\frac{2\pi}{N}d(q-l_\nu^{(i)})} \tag{25}$$

When $k = d$, equation (25) simplifies to

$$\left[\boldsymbol{R}_{\boldsymbol{\theta}_d,\boldsymbol{\theta}_d}^{(i)}\right]_{\nu,\nu} = \sigma_{l_\nu^{(i)}}^{(i)2}\sum_{m=-N_\beta+1}^{N_\beta-1} \rho_m e^{-j\frac{2\pi}{N}dm}$$
$$\times \frac{1}{N}\sum_{p=0}^{N_\beta-1} \beta_p\beta_{p-m}^* \alpha_{p-l_\nu^{(i)}}\alpha_{p-m-l_\nu^{(i)}}^* \tag{26}$$

The values $\{[\boldsymbol{R}_{\boldsymbol{\theta}_d,\boldsymbol{\theta}_d}^{(i)}]_{\nu,\nu}\}_{d=-D}^D$ can be recognized as samples of the pulse-shaped Doppler spectrum of the νth active tap. The pulses $\{\alpha_p\}$ and $\{\beta_p\}$, designed to suppress ICI beyond a radius of D subcarriers, act via the second summation in (26) to squeeze the un-shaped Doppler spectrum $\{\sigma_{l_\nu^{(i)}}^{(i)2}\sum_m \rho_m e^{-j\frac{2\pi}{N}dm}\}_{d=0}^{N-1}$ into the (truncated) pulse-shaped Doppler spectrum $\{[\boldsymbol{R}_{\boldsymbol{\theta}_d,\boldsymbol{\theta}_d}^{(i)}]_{\nu,\nu}\}_{d=-D}^D$.

Thus, we use pulse shaping to restrict the degrees of temporal channel variation (per MCM symbol) from N to $2D+1$,
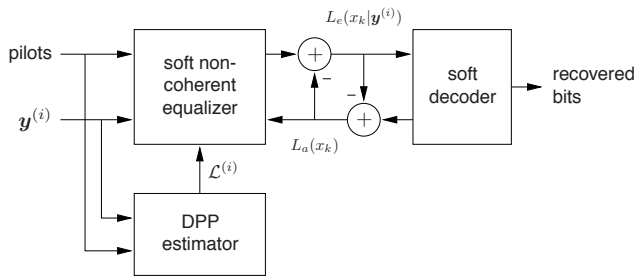
Fig. 1. Receiver structure.

and we use a BEM to restrict the degrees of spectral channel variation from N to N_a. The resulting channel representation $\boldsymbol{\theta}^{(i)} \in \mathbb{C}^{(2D+1)N_a}$ has an autocorrelation matrix $\boldsymbol{R}_{\boldsymbol{\theta}}^{(i)}$ that will be full rank under properly designed pulses (e.g., [15]).

III. NONCOHERENT SOFT EQUALIZATION

As illustrated in Fig. 1, the receiver consists of a soft noncoherent equalizer and a soft decoder, connected in a "turbo" configuration, as well as a delay-power profile (DPP) estimator. The DPP estimator uses the observations and pilots to estimate the active-tap indices $\mathcal{L}^{(i)}$, as will be described in Section IV. The equalizer uses the observations $\boldsymbol{y}^{(i)}$, as well as any *a priori* information provided by the decoder, to generate soft information on the coded bits $\boldsymbol{x}^{(i)} := [\underline{\boldsymbol{x}}_0^{(i)T}, \ldots, \underline{\boldsymbol{x}}_{N_s-1}^{(i)T}]^T$, leveraging its knowledge of the pilot symbols and statistical channel structure, including $\mathcal{L}^{(i)}$. The decoder then uses the soft equalizer outputs (from possibly many MCM-symbols) to refine the soft information on the coded bits, leveraging its knowledge of the code structure. After a sufficient number of turbo iterations, the decoder outputs a hard estimate of the information bits.

In this section, we describe the proposed noncoherent soft equalizer, where the soft information takes the form of log-likelihood ratios (LLRs) on coded bits. Given the observation $\boldsymbol{y}^{(i)}$ and the *a priori* LLRs (which may have been refined by the decoder), the soft equalizer generates LLRs for each of the coded bits in $\boldsymbol{x}^{(i)}$. The equalizer is "noncoherent" in that it treats the channel realization $\boldsymbol{\theta}^{(i)}$ as unknown. However, it is assumed to know the distributions of $\boldsymbol{\theta}^{(i)}$ and $\boldsymbol{w}^{(i)}$, which are taken to be[4] $\mathcal{CN}(\boldsymbol{0}, \boldsymbol{R}_{\boldsymbol{\theta}}^{(i)})$ and $\mathcal{CN}(\boldsymbol{0}, \sigma^2 \boldsymbol{I})$, respectively. In deriving our algorithm, we assume a perfect estimate of the active-tap locations $\mathcal{L}^{(i)}$. In addition, we make the mild assumption that the autocovariance matrix $\boldsymbol{R}_{\boldsymbol{\theta}}^{(i)}$ (whose form can be inferred from (16) and (25)) is full rank. Because the equalizer processing is invariant to the MCM-symbol index i, we suppress the superscript notation in the remainder of Section III.

A. LLR Approximation

The LLR of coded bit x_j given $\boldsymbol{y}$, defined as follows for $j \in \{0, \ldots, N_sQ - 1\}$:

$$L(x_j|\boldsymbol{y}) := \ln \frac{P[x_j = 1|\boldsymbol{y}]}{P[x_j = 0|\boldsymbol{y}]}, \qquad (27)$$

can be written in the form [25]

$$L(x_j|\boldsymbol{y}) = \ln \frac{\sum_{\boldsymbol{x}:x_j=1} p(\boldsymbol{y}|\boldsymbol{x}) \exp \boldsymbol{l}^T \boldsymbol{x}}{\sum_{\boldsymbol{x}:x_j=0} p(\boldsymbol{y}|\boldsymbol{x}) \exp \boldsymbol{l}^T \boldsymbol{x}}, \qquad (28)$$

for $\boldsymbol{l} := [L_a(x_0), \ldots, L_a(x_{N_sQ-1})]^T$, where $L_a(x_j) := \ln P[x_j = 1]/P[x_j = 0]$ denotes the *a priori* LLR of x_j. The use of the metric

$$\mu(\boldsymbol{x}) := \ln p(\boldsymbol{y}|\boldsymbol{x}) + \boldsymbol{l}^T \boldsymbol{x} \qquad (29)$$

allows the "extrinsic" LLR $L_e(x_j|\boldsymbol{y}) := L(x_j|\boldsymbol{y}) - L_a(x_j)$ to be written as

$$L_e(x_j|\boldsymbol{y}) = \ln \frac{\sum_{\boldsymbol{x}:x_j=1} \exp \mu(\boldsymbol{x})}{\sum_{\boldsymbol{x}:x_j=0} \exp \mu(\boldsymbol{x})} - L_a(x_j). \qquad (30)$$

Computing $L_e(x_j|\boldsymbol{y})$ via (30) is impractical because it requires 2^{N_sQ} evaluations of $\mu(\boldsymbol{x})$. However, as suggested in [25], the extrinsic LLR $L_e(x_j|\boldsymbol{y})$ can be approximated as

$$L_e(x_j|\boldsymbol{y}) \approx \max_{\boldsymbol{x}\in\mathcal{X}\cap\{\boldsymbol{x}:x_j=1\}} \mu(\boldsymbol{x}) - \max_{\boldsymbol{x}\in\mathcal{X}\cap\{\boldsymbol{x}:x_j=0\}} \mu(\boldsymbol{x}) - L_a(x_j), (31)$$

using the "max-log" approximation $\ln \sum_{\boldsymbol{x}:x_j=1} \exp \mu(\boldsymbol{x}) \approx \max_{\boldsymbol{x}:x_j=1} \mu(\boldsymbol{x})$ and subsequently restricting the maximization search space to the "most important" bit sequences $\mathcal{X}$.

The model (17), in conjunction with our Rayleigh fading assumption, yields $\boldsymbol{y}|\boldsymbol{x} \sim \mathcal{CN}(\boldsymbol{0}, \boldsymbol{A}\boldsymbol{R}_{\boldsymbol{\theta}}\boldsymbol{A}^H + \sigma^2 \boldsymbol{I}_N)$, where from (18) we recall that $\boldsymbol{A}$ depends on the coded bits $\boldsymbol{x}$ through the (D-shifted) scalar symbols $\bar{\boldsymbol{c}}$. With $\boldsymbol{\Phi} := \boldsymbol{A}\boldsymbol{R}_{\boldsymbol{\theta}}\boldsymbol{A}^H + \sigma^2 \boldsymbol{I}_N$ we find $\ln p(\boldsymbol{y}|\boldsymbol{x}) = -\boldsymbol{y}^H \boldsymbol{\Phi}^{-1} \boldsymbol{y} - \ln(\pi^N \det \boldsymbol{\Phi})$, allowing the metric to be written as

$$\mu(\boldsymbol{x}) = -\boldsymbol{y}^H \boldsymbol{\Phi}^{-1} \boldsymbol{y} - \ln(\pi^N \det \boldsymbol{\Phi}) + \boldsymbol{l}^T \boldsymbol{x}. \qquad (32)$$

B. LLR Evaluation via Tree Search

Because direct evaluation of (32) requires $\mathcal{O}(N_s^3)$ operations and there are 2^{N_sQ} candidate bit sequences to evaluate, the computation of $\{\mu(\boldsymbol{x})\}_{\boldsymbol{x}\in\mathcal{X}}$ remains computationally challenging. In the practical approach of [26], the partial metric

$$\mu_k(\boldsymbol{x}_k) := \ln p(\boldsymbol{y}_k|\boldsymbol{x}_k) + \boldsymbol{l}_k^T \boldsymbol{x}_k \qquad (33)$$

is evaluated *sequentially* (i.e., in the order $\mu_0(\boldsymbol{x}_0), \mu_1(\boldsymbol{x}_1), \ldots, \mu_{N_s-1}(\boldsymbol{x}_{N_s-1})$) using M possibilities of each partial bit vector $\boldsymbol{x}_k$, where here $\boldsymbol{l}_k := [\underline{\boldsymbol{l}}_0^T, \ldots, \underline{\boldsymbol{l}}_k^T]^T$ and $\underline{\boldsymbol{l}}_i := [L(x_{iQ}), \ldots, L(x_{iQ+Q-1})]^T$. To choose the M possibilities of $\boldsymbol{x}_k$, all one-symbol extensions of the M "most important" partial bit vectors $\boldsymbol{x}_{k-1}$ are examined, and only the M extensions yielding the largest partial metrics $\mu_k(\boldsymbol{x}_k)$ are retained. In other words, the M-algorithm[5] [27], a breadth-first suboptimal tree-search algorithm, is applied to compute $\{\mu(\boldsymbol{x})\}_{\boldsymbol{x}\in\mathcal{X}'}$ for $\mathcal{X}' \approx \mathcal{X}$. Since $\mathcal{X}' \cap \{\boldsymbol{x} : x_k = 1\}$ or $\mathcal{X}' \cap \{\boldsymbol{x} : x_k = 0\}$ can be empty for some k, the LLRs must be clipped to prevent them from being infinite. The choice of clipping threshold is discussed in [26].

As we have shown in [20], the metric $\mu_k([\boldsymbol{x}_{k-1}; x_k])$ can be computed from $\mu_{k-1}(\boldsymbol{x}_{k-1})$ using only $\mathcal{O}(D^2 N_a^2)$ operations, so that $\{\mu(\boldsymbol{x})\}_{\boldsymbol{x}\in\mathcal{X}'}$ can be evaluated using only

---

[4]Since the noise $\boldsymbol{w}^{(i)}$ is circular white Gaussian under a rectangular demodulation pulse (i.e., $\beta_n = 1$ for $n \in \{0, \ldots, N-1\}$ and $\beta_n = 0$ otherwise), we assume a rectangular pulse in the sequel.

[5]Other types of tree search could also be applied. However, the M-algorithm is convenient because its complexity is invariant to both channel realization and SNR.

TABLE I
FAST COMPUTATION OF $\mu(\boldsymbol{x})$.

$$
\begin{aligned}
&\text{set } \{\mu_{-1}(\boldsymbol{x}_{-1}), \ \boldsymbol{\Sigma}_{-1}^{-1}, \ \hat{\boldsymbol{\theta}}_{-1}\} := \{\ln \sigma^{-2}, \ \sigma^{-2}\boldsymbol{R_\theta}, \ \boldsymbol{0}\}; \\
&\text{for } k = 0, 1, 2, \dots, N-1, \\
&\quad \boldsymbol{a}_k = [\bar{c}_k \boldsymbol{b}_k^H, \cdots, \bar{c}_{k-N_a+1} \boldsymbol{b}_k^H]^H; \\
&\quad \boldsymbol{d}_k = \boldsymbol{\Sigma}_{k-1}^{-1} \boldsymbol{a}_k; \\
&\quad \alpha_k = (1 + \boldsymbol{a}_k^H \boldsymbol{d}_k)^{-1}; \\
&\quad \boldsymbol{\Sigma}_k^{-1} = \boldsymbol{\Sigma}_{k-1}^{-1} - \alpha_k \boldsymbol{d}_k \boldsymbol{d}_k^H; \\
&\quad e_k = r_k - \boldsymbol{a}_k^H \hat{\boldsymbol{\theta}}_{k-1}; \\
&\quad \mu_k(\boldsymbol{x}_k) = \mu_{k-1}(\boldsymbol{x}_{k-1}) - \frac{\alpha_k}{\sigma^2}|e_k|^2 - \ln(\pi \alpha_k) + \underline{\boldsymbol{l}}_k^T \underline{\boldsymbol{x}}_k; \\
&\quad \hat{\boldsymbol{\theta}}_k = \hat{\boldsymbol{\theta}}_{k-1} + \alpha_k e_k \boldsymbol{d}_k; \\
&\text{end}
\end{aligned}
$$

Fig. 2. Illustration of pilot pattern with $N = 32$, $P = 4$, $K = 2$, $N_p = 8$, and $D = 1$. The columns represent $\bar{\boldsymbol{c}}^{(i-P+2)}, \dots, \bar{\boldsymbol{c}}^{(i+2P-3)}$, respectively.

$\mathcal{O}(NM2^Q D^2 N_a^2)$ operations. In particular, by writing the partial metric (33) in the form of (32), we find

$$
\mu_k(\boldsymbol{x}_k) = -\boldsymbol{y}_k^H \boldsymbol{\Phi}_k^{-1} \boldsymbol{y}_k - \ln(\pi^{k+1} \det \boldsymbol{\Phi}_k) + \boldsymbol{l}_k^T \boldsymbol{x}_k, \quad (34)
$$

where $\boldsymbol{\Phi}_k := \boldsymbol{A}_k \boldsymbol{R_\theta} \boldsymbol{A}_k^H + \sigma^2 \boldsymbol{I}_{k+1}$. Table I outlines a fast sequential algorithm for the computation of $\mu(\boldsymbol{x})$ which can be seen to require $N_s((2D+1)^2 N_a^2 + 3(2D+1)N_a + 7)$ multiplications. The quantity $\hat{\boldsymbol{\theta}}_k$ in Table I denotes the MMSE estimate of $\boldsymbol{\theta} \in \mathbb{C}^{(2D+1)N_a}$ conditioned on $\boldsymbol{x}_k$ and *not* an estimate of the quantity $\boldsymbol{\theta}_d \in \mathbb{C}^{N_a}$ from (14). The complexity of our soft equalizer is thus *linear* in the block length N and *quadratic* in the number of active channel parameters DN_a.

C. Incorporating Pilot Symbols

Due to the quadratic nature of the metric $\mu(\boldsymbol{x})$, the previously described noncoherent equalizer inherits a gain/phase ambiguity which can be resolved through the use of a single pilot symbol (e.g., [28]). The judicious use of *several* pilots, however, can dramatically improve the performance of suboptimal tree-search. In our case, this would allow the M-algorithm to be used with relatively small M. Intuitively, with more pilots, the M-algorithm can compute a better estimate of $\boldsymbol{\theta}$ before it is forced to prune paths.

Note that the following simple modification of the M-algorithm suffices to handle the presence of pilot/guard symbols within $\bar{\boldsymbol{c}}$: When the M-algorithm encounters a known symbol, each surviving path is given a single (rather than 2^Q-ary) extension with a zero-valued LLR. If symbols outside of $\bar{\boldsymbol{c}}$ are known (e.g., pilot subcarriers in neighboring MCM-symbols), we suggest using them to compute an MMSE estimate $\hat{\boldsymbol{\theta}}_{-1} \neq \boldsymbol{0}$ to use in Table I. After the first turbo iteration, soft or hard decoder outputs can also be used to calculate $\hat{\boldsymbol{\theta}}_{-1}$.

IV. TRACKING SPARSITY

In this section, we present an efficient means of learning the active-tap locations $\mathcal{L}^{(i)}$ and compensating for the fact that, in practice, "inactive" taps are non-zero (but small).

A. Active-Tap Identification

To estimate the locations of active taps, we compute a pilot-based minimum mean-squared error (MMSE) estimate of the non-compressed BEM coefficient vector
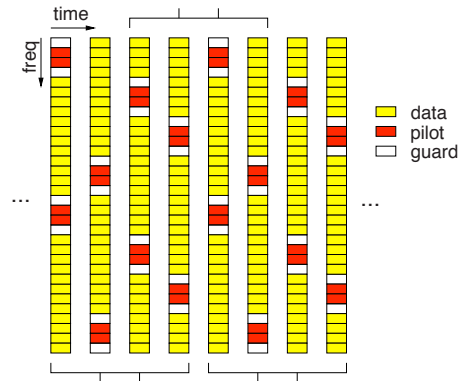
$\breve{\boldsymbol{\theta}}^{(i)} := [\breve{\boldsymbol{\theta}}_{-D}^{(i)T}, \dots, \breve{\boldsymbol{\theta}}_D^{(i)T}]^T$ and from that estimate the DPP $\{\sigma_l^{(i)2}\}_{l=0}^{N_h-1}$ as follows.

$$
\widehat{\sigma_l^{(i)2}} = \sum_{d=-D}^{D} \left| [\breve{\boldsymbol{\theta}}_d^{(i)}]_l \right|^2. \quad (35)
$$

Note that this approach permits accurate DPP estimation even when the channel gain $h_{n,l}^{(i)}$ varies significantly over the MCM-symbol interval. Once the DPP has been estimated, we set[6] $\mathcal{L}^{(i)}$ as the largest N_a indices of the DPP. Note that the ability to assign $\mathcal{L}^{(i)}$ directly from the DPP is a consequence of our BEM's orthogonality (i.e., $\boldsymbol{F}$). Without BEM orthogonality, estimating $\mathcal{L}^{(i)}$ becomes much more complicated (e.g., [23]).

As illustrated in Fig. 2, our pilot pattern employs $N_p = N/P$ pilot/guard subcarriers per MCM-symbol and repeats after every P MCM-symbols. Each MCM-symbol contains $K \geq 1$ pilot clusters, where each cluster is comprised of $N_p/K - 2D$ non-zero pilots with D zero-valued guards on either edge. The cluster locations are staggered so that each subcarrier is used in a cluster exactly once every P MCM-symbols. Note that, on average, $\frac{P-1}{P}$ subcarriers are used for data. We experiment with different choices of K in Section V.

The pilots play a twofold[7] role. First, as discussed in Section III-C, they have the potential to significantly improve the complex/performance tradeoff of suboptimal tree-search. Second, they facilitate the tracking of active taps $\mathcal{L}^{(i)}$. Recall that DPP sparsity can lead to significant reductions in equalization complexity since the latter is quadratic in the number of modeled taps (i.e., $N_a = |\mathcal{L}^{(i)}|$). The guards also play a twofold role. First, as described in Section II-C, they facilitate tree-search by making the ICI channel (17) appear causal. Second, they ensure that $N_p - 2KD$ subcarriers in $\boldsymbol{y}^{(i)}$ will be free of interference from unknown data, thereby improving the quality of pilot-based estimates of $\mathcal{L}^{(i)}$.

[6] Note that this approach yields a fixed complexity; if a fixed performance was more important, one could set $\mathcal{L}^{(i)}$ to be the indices of DPP values that lie above a threshold.

[7] Note that pilots could also be used for adjustment of *large* timing clock offsets and carrier frequency offsets. For example, the receiver's sampling and carrier frequencies could be adjusted so that the support of the measured delay/Doppler profile stays close to the origin. There is no need to compensate for small timing/carrier offsets, though, since they are subsumed by the doubly dispersive channel.

We now detail our pilot-based DPP estimation procedure, assuming power-of-two P. At even symbol indices i, we use the pilot-only subcarriers in $\{\boldsymbol{y}^{(i)}, \ldots, \boldsymbol{y}^{(i+P-1)}\}$ to jointly estimate the channel vectors $\{\boldsymbol{\breve{\theta}}^{(i+P/4)}, \ldots, \boldsymbol{\breve{\theta}}^{(i+3P/4-1)}\}$. Here, estimates for the $P/4$ left and right "edge" vectors are not attempted because we anticipate that they would be unreliable. However, since estimation is performed at every even symbol index i, all channel vectors will eventually be estimated. (See Fig. 2 for a $P = 4$ example.) Notice that a total of $P(N_p - 2KD) = N - 2PKD$ scalar observations are used to estimate $\frac{P}{2}(2D+1)N_h$ scalar BEM coefficients during every other MCM-symbol index. Since MMSE estimation is implemented by multiplication with a (fixed and known) $\frac{P}{2}(2D+1)N_h \times (N - 2PDK)$ matrix, the cost of DPP estimation is only $\frac{P}{4}(2D+1)N_h(N-2PDK)$ multiplications per MCM-symbol. Recalling Section III-B, this cost is small relative to that of iterative noncoherent soft equalization.

The MMSE estimator matrix can be designed as follows. Say that we collect the pilot-only observations from $\{\boldsymbol{y}^{(i)}, \ldots, \boldsymbol{y}^{(i+P-1)}\}$ into the vector $\underline{\boldsymbol{y}}^{(i)} \in \mathbb{C}^{N-2PKD}$ and the corresponding noise samples $\{w_k\}$ into the vector $\underline{\boldsymbol{w}}^{(i)}$. Then, considering (17) with non-compressed coefficients $\boldsymbol{\breve{\theta}}^{(i)}$, we can write

$$\underline{\boldsymbol{y}}^{(i)} = \underline{\boldsymbol{A}}\underline{\boldsymbol{\breve{\theta}}}^{(i)} + \underline{\boldsymbol{w}}^{(i)}, \qquad (36)$$

where $\underline{\boldsymbol{A}}$ is a block-diagonal pilot matrix (with P blocks) and $\underline{\boldsymbol{\breve{\theta}}}^{(i)} := [\boldsymbol{\breve{\theta}}^{(i)T}, \ldots, \boldsymbol{\breve{\theta}}^{(i+P-1)T}]^T$. The MMSE estimate of $\underline{\boldsymbol{\breve{\theta}}}^{(i)}$ from $\underline{\boldsymbol{y}}^{(i)}$ is then

$$\underline{\boldsymbol{\hat{\theta}}}^{(i)} = \boldsymbol{R}_{\underline{\breve{\theta}}}\underline{\boldsymbol{A}}^H(\underline{\boldsymbol{A}}\boldsymbol{R}_{\underline{\breve{\theta}}}\underline{\boldsymbol{A}}^H + \sigma^2 \boldsymbol{I})^{-1}\underline{\boldsymbol{y}}^{(i)}, \qquad (37)$$

where $\boldsymbol{R}_{\underline{\breve{\theta}}}$ denotes the autocovariance matrix for $\underline{\boldsymbol{\breve{\theta}}}^{(i)}$, which can be constructed from the WSSUS model (25) under an *a priori* uniform DPP, i.e., $\sigma_{l_\nu^{(i)}}^{(i)2} = N_h^{-1}$ for $\nu \in \{0, \ldots, N_h - 1\}$ and $l_\nu^{(i)} = \nu$. Finally, DPP estimates of $\{\sigma_l^{(i+P/4)2}, \ldots, \sigma_l^{(i+3P/4-1)2}\}_{l=0}^{N_h-1}$ are computed via (35).

B. Residual Tap Compensation

Because non-active channel taps are ignored by the noncoherent equalizer, they have the effect of contributing additional noise. Since the size and number of non-active channel taps can vary, so can the power of the additional noise. Thus, it should be tracked for use by the equalizer. Fortunately, doing so is relatively easy. For example, after the noncoherent sequence detection algorithm has estimated $\boldsymbol{A}^{(i)}$ and $\boldsymbol{\theta}^{(i)}$ in (17), the energy of the residual interference $\boldsymbol{\hat{w}}^{(i)} := \boldsymbol{y}^{(i)} - \boldsymbol{\hat{A}}^{(i)}\boldsymbol{\hat{\theta}}^{(i)}$ can be used as an estimate of the effective noise power $\sigma^{(i)2}$. This estimate could then be employed for noncoherent equalization of the $(i+1)^{th}$ MCM-symbol, since the sparsity is not expected to change significantly from one MCM-symbol to the next.

V. NUMERICAL RESULTS

Numerical tests of the proposed multicarrier system were conducted using MATLAB, using active channel coefficients with Rayleigh-fading gains and time-varying delays.

A. Setup

Two types of channel were considered, a "perfectly sparse" channel and a "sparse" channel; the latter aims to be realistic while the former is useful as a reference. The impulse response of the "perfectly sparse" channel had $N_c = 5$ nonzero fading coefficients spread over $N_h = 50$ chip intervals. The temporal trajectories of each of the N_c coefficients were independently generated from a zero-mean circular[8] Gaussian random processes with a Gaussian-shaped power spectrum, where $f_D T_c = 0.002$ was chosen for the single-sided normalized Doppler spread. The delay power profile (DPP) was exponential, i.e., the energy of the Gaussian process at chip delay l was $\sigma_l^2 = C\exp(-\frac{\ln 4}{N_h}l)$, where C was chosen to make the channel energy-preserving. Our choice of $\{f_D T_c, N_h\}$ corresponds to, for example, Doppler spread 30 Hz and delay spread 7 ms if the transmission bandwidth was $\frac{1}{T_c} = 7.5$ kHz, which match the surf-zone channel from [4]. To generate the more realistic "sparse" channel model, 2% of the active-tap energy was leaked into the inactive taps. This was accomplished by convolving the "perfectly sparse" impulse response $\{h_{n,l}\}_{l=0}^{N_h-1}$, at each time n, with the truncated sinc sequence $[-0.0721, 0.0739, 0.9893, 0.0739, -0.0721]$.

To model a time-varying DPP, the discrete delays of the active taps were varied in time as follows. While the delays of the first and second taps were fixed at 2 and 9 chips, the delay of the third changed from 14 to 18 chips with a period of 225 MCM-symbol intervals. Furthermore, the delay of the fourth changed from 21 to 26 chips, and then back, with a period of 60 MCM-symbol intervals, and the delay of the fifth changed from 32 to 47 chips, and then back, with a period of 60 MCM-symbol intervals. Thus, it can be seen that the delay spread of the "sparse" channel was $N_h = 50$. As a consequence of the time-varying tap delays, the effective Doppler spread is actually larger than $f_D T_c = 0.002$.

At the transmitter, information bits were coded via rate-$R = \frac{1}{2}$ irregular low density parity check (LDPC) codes with average column-weight 3, generated via the publicly available software [29]. The coded bits were then mapped to BPSK symbols (i.e., $Q = 1$) and partitioned into data blocks of length $N_s = N - N_p$, each of which was merged with $N_p = 32$ pilot/guard symbols to form an MCM-symbol of length $N = 128$. We used random BPSK pilots arranged as in Fig. 2 with $P = 4$, $D = 1$, and $K = 1$ (unless otherwise noted). So that each codeword spanned exactly $J = 128$ MCM-symbol intervals, $(JQN_s, RJQN_s)$-LDPC codes were employed. For the MCM pulses $\{\alpha_n\}$ and $\{\beta_n\}$, we used the "transmitter optimized max-SINR" design from [15], which specifies a smooth modulation pulse of length $N_\alpha = 1.5N$ and a rectangular demodulation pulse of length $N_\beta = N$. Since we employed no MCM guard interval, our modulation efficiency (taking the pilots/guards into account) was 0.75 symbols/sec/Hz.

The receiver employed an ICI radius of $D = \lceil f_D T_c N \rceil = 1$ and used $N_a = 10$ active taps in its BEM. For noncoherent soft equalization, the LLR clipping threshold was set at 3.0 and the M-algorithm used a search breadth of $M = 32$. A maximum

---

[8]Here, and throughout the paper, we refer to the complex-baseband equivalent model of the channel.
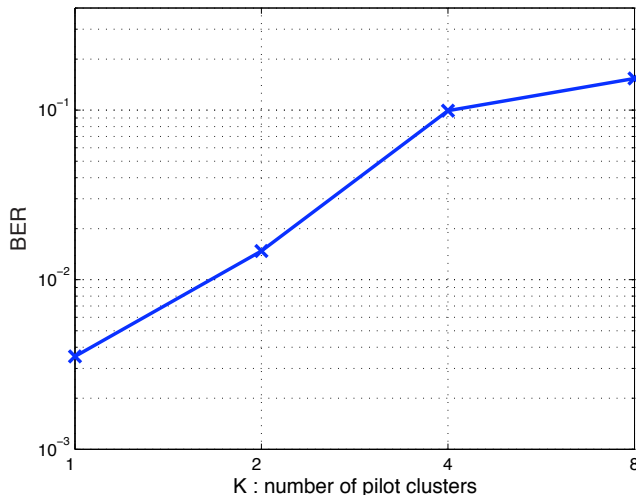
Fig. 3. BER versus number of pilot clusters for the "sparse" channel at $E_b/N_o = 11.5$ dB.

Fig. 4. BER versus SNR for the "perfectly sparse" channel, where non-significant taps have zero energy. The noncoherent soft equalizer is compared to coherent soft equalizer with genie-estimated $\boldsymbol{\theta}^{(i)}$ for both true and estimated $\mathcal{L}^{(i)}$.

Fig. 5. BER versus SNR for the "sparse" channel, where non-significant taps have small but non-zero energy. The noncoherent soft equalizer is compared to coherent soft equalizer with genie-estimated $\boldsymbol{\theta}^{(i)}$ for both true and estimated $\mathcal{L}^{(i)}$.

of 60 sum-product decoding iterations were allowed, while a maximum of 8 turbo (i.e., equalization/decoding) iterations were allowed. Note, however, that decoder and turbo iterations are terminated as soon as the LDPC decoder senses that the bits have been decoded without error (which usually happens very quickly).

B. BER versus Number of Pilot Clusters K

We first investigated the bit error rate (BER) versus the number of pilot clusters K for fixed N and P. Intuitively, there are two competing notions for the choice of K. On one hand, since each cluster includes $2D$ zero-valued guards (to prevent interference from the unknown data subcarriers) in addition to $N_p/K - 2D$ non-zero pilots, the total number of non-zero pilots per MCM symbol is $N_p - 2KD$, which increases as K decreases, suggesting better channel estimates. But, on the other hand, as K decreases, the pilot subcarriers are located farther from the subcarrier locations at which the channel must be estimated, suggesting worse channel estimates. The theoretically optimum choice of K (e.g., [17], [30]) is only known for simplified (e.g., non-sparse) channel models and MSE-minimization (rather than coded-BER minimization) and thus falls short of being accurate here.

In Fig. 3, we plot the BER versus $K \in \{1, 2, 4, 8\}$. Since we fix $N_p = 32$, these values of K correspond to cluster sizes of $\{32, 16, 8, 4\}$, respectively. Figure 3 shows that, here, $K = 1$ yields minimum BER, i.e., that one large cluster outperforms many smaller clusters.

C. BER versus SNR

Next we investigated BER versus E_b/N_o, i.e., the ratio of energy-per-information-bit to noise power-spectral-density. (Note that pilot/guards to not contribute to the information-bit energy.) In addition to simulating the BER of the proposed soft noncoherent receiver, we also simulated the BER of several genie-aided reference receivers. In one reference receiver, we replace our soft noncoherent equalizer with the soft *coherent* equalizer from [26] that uses an MMSE estimate of $\boldsymbol{\theta}^{(i)}$ computed under the assumption that, in addition to the pilot/guards, *all data subcarriers are known for the purpose of estimating* $\boldsymbol{\theta}^{(i)}$. Notice that this "genie-aided-$\hat{\boldsymbol{\theta}}$ coherent reference" upper bounds the performance of any noncoherent equalizer with a bound tighter than that of coherent equalization under *perfect* channel knowledge. Since, however, both the noncoherent and genie-aided-$\hat{\boldsymbol{\theta}}$ equalizers still need to track the active coefficients $\mathcal{L}^{(i)}$, we consider these two schemes with perfectly known $\mathcal{L}^{(i)}$ as additional references.
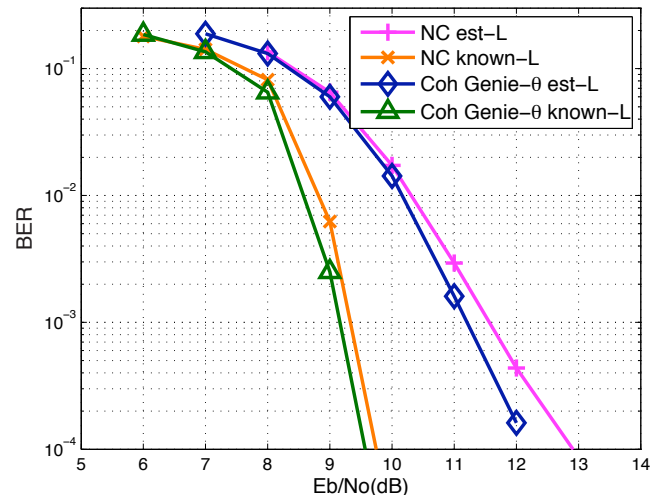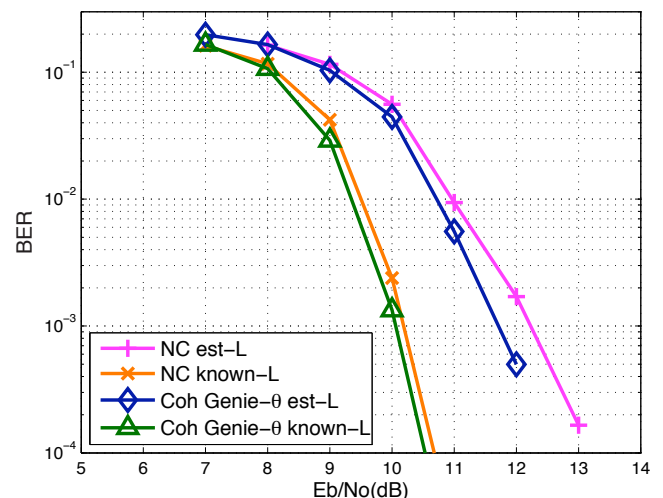
Fig. 4 shows BER versus E_b/N_o for the "perfectly sparse" channel. The performance of the proposed soft noncoherent receiver shows about 0.25 dB SNR loss (at $10^{-2.5}$ BER) relative to the genie-aided-$\hat{\boldsymbol{\theta}}$ coherent receiver that estimates
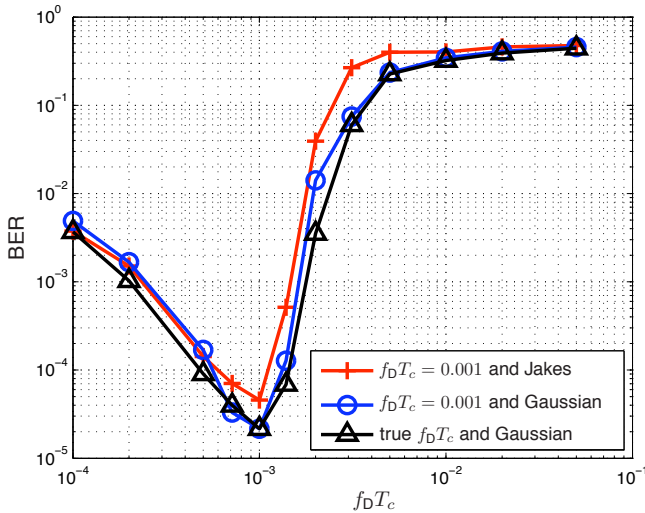
Fig. 6. BER versus true $f_D T_c$ for matched and mismatched noncoherent equalizers using the "sparse" channel at $E_b/N_o = 11.5$ dB.

$\mathcal{L}^{(i)}$ and about 2 dB relative to the genie-aided-$\hat{\boldsymbol{\theta}}$ coherent receiver with known $\mathcal{L}^{(i)}$. Thus, most of the loss is due to imperfect estimation of $\mathcal{L}^{(i)}$. Not surprisingly, the $\mathcal{L}^{(i)}$-estimates can be shown to improve with the number of pilots.

Fig. 5 shows BER versus E_b/N_o for the "sparse" channel. Here again, the proposed noncoherent receiver performs about 0.3 dB worse (at $10^{-2.5}$ BER) than the genie-aided-$\boldsymbol{\theta}$ reference that estimates $\mathcal{L}^{(i)}$ and about 2 dB worse than the genie-aided-$\boldsymbol{\theta}$ reference that knows $\mathcal{L}^{(i)}$ perfectly.

D. Robustness to Assumed Doppler Statistics

Finally we investigate the effect of a mismatch between the true and assumed Doppler statistics $\{\rho_m\}$. In particular, we plot BER performance versus Doppler spread $f_D T_c$ for a receiver which knows $f_D T_c$ and the Doppler spectrum, and for two mismatched receivers: one which assumes $f_D T_c = 0.001$ and the correct (i.e., Gaussian) spectrum, and the other which assumes $f_D T_c = 0.001$ and Jakes spectrum [31]. Figure 6 shows that mismatch in $f_D T_c$ and Doppler spectrum is handled quite well; only a small BER increase above the matched receiver is evident.

The behavior of the matched receiver in Fig. 6 can be understood as follows. As $f_D T_c$ increases, the BER-versus-SNR curves get steeper as a result of increased Doppler diversity, but shift to the right as a result of the fact that the channel is more difficult to estimate. So, as $f_D T_c$ increases up to 0.001, BER at $E_b/N_o = 11.5$ dB improves because the effects of steepness dominate those of shift. But, as $f_D T_c$ increases beyond 0.001, BER at $E_b/N_o = 11.5$ dB degrades because the effects of shift dominate those of steepness. By raising E_b/N_o, better BER would be seen at high $f_D T_c$.

VI. CONCLUSION

In this paper we presented a novel multicarrier strategy for communication over UACs with simultaneously large delay and Doppler spreads. A multicarrier scheme employing a

smooth transmission pulse was chosen to transform a time-varying ISI span of fifty taps to an ICI span of three taps. Careful design of the pulse eliminated the need for a bandwidth-wasting cyclic (or zero) prefix. A turbo receiver, which passes soft bit information between a noncoherent equalizer and an off-the-shelf decoder, was then described. The complexity of the noncoherent equalizer, which assumes knowledge of the channel's statistics but not its realizations, is relatively low due to the use of suboptimal tree search and the leveraging of sparsity in the channel's delay-power profile. Although the noncoherent equalizer can function with only a single pilot subcarrier, a more extensive pilot pattern is proposed to track the (time-varying) sparsity profile as well as to reduce the complexity of near-optimal tree search. Because the metric used for noncoherent equalization has a fast recursive update, equalization requires only $\approx M|\mathcal{S}|(2D+1)^2 N_a^2$ multiplications per subcarrier, where M is the tree-search parameter (e.g., $M = 32$ for our simulations), $|\mathcal{S}|$ is the subcarrier alphabet size, $(2D+1)$ is the ICI span, and N_a is the number of active delays. Simulations with highly spread channels (e.g., $f_D T_h = 0.1$) showed that the performance of the proposed noncoherent algorithm was about 2 dB away from coherent detection using a genie-estimated channel. Simulations also showed that the proposed technique is relatively insensitive to mismatch of the assumed Doppler spectrum.

REFERENCES

[1] D. Brady and J. C. Preisig, "Underwater acoustic communications," in *Wireless Communications: Signal Processing Perspectives* (H. V. Poor and G. W. Wornell, eds.), ch. 8, pp. 330–379, Prentice-Hall, 1998.

[2] M. Stojanovic, J. A. Catipovic, and J. G. Proakis, "Phase-coherent digital communications for underwater acoustic channels," *IEEE J. Oceanic Eng.*, vol. 19, pp. 100–111, Jan. 1994.

[3] J. C. Preisig, "Performance analysis of adaptive equalization for coherent acoustic communications in the time-varying ocean environment," *J. Acoust. Soc. Am.*, vol. 118, pp. 263–278, July 2005.

[4] J. C. Preisig and G. Deane, "Surface wave focusing and acoustic communications in the surf zone," *J. Acoust. Soc. Am.*, vol. 116, pp. 2067–2080, Oct. 2004.

[5] B. Li, S. Zhou, M. Stojanovic, and L. Freitag, "Pilot-tone based ZP-OFDM demodulation for an underwater acoustic channel," in *Proc. IEEE OCEANS*, Sept. 2006.

[6] M. Stojanovic, "Low complexity OFDM detector for underwater acoustic channels," in *Proc. IEEE OCEANS*, Sept. 2006.

[7] A. K. Morozov and J. C. Preisig, "Underwater acoustic communications with multi-carrier modulation," in *Proc. IEEE OCEANS*, Sept. 2006.

[8] Y. Li and L. J. Cimini, Jr., "Bounds on the interchannel interference of OFDM in time-varying impairments," *IEEE Trans. Commun.*, vol. 49, pp. 401–404, Mar. 2001.

[9] R. Raheli, A. Polydoros, and C. K. Tzou, "Per-survivor processing: A general approach to MLSE in uncertain environments," *IEEE Trans. Commun.*, vol. 43, pp. 354–364, Feb./Mar./Apr. 1995.

[10] B. Li, S. Zhou, M. Stojanovic, L. Freitag, and P. Willett, "Non-uniform Doppler compensation for zero-padded OFDM over fast-varying underwater acoustic channel," in *Proc. IEEE OCEANS*, June 2007.

[11] B. Le Floch, M. Alard, and C. Berrou, "Coded orthogonal frequency division multiplex," *Proc. IEEE*, vol. 83, pp. 982–996, June 1995.

[12] W. Kozek and A. F. Molisch, "Nonorthogonal pulseshapes for multi-carrier communications in doubly dispersive channels," *IEEE J. Select. Areas Commun.*, vol. 16, pp. 1579–1589, Oct. 1998.

[13] T. Strohmer and S. Beaver, "Optimal OFDM design for time-frequency dispersive channels," *IEEE Trans. Commun.*, vol. 51, pp. 1111–1122, July 2003.

[14] K. Liu, T. Kadous, and A. M. Sayeed, "Orthogonal time-frequency signaling over doubly dispersive channels," *IEEE Trans. Inform. Theory*, vol. 50, pp. 2583–2603, Nov. 2004.

[15] S. Das and P. Schniter, "Max-SINR ISI/ICI-shaping multi-carrier communication over the doubly dispersive channel," *IEEE Trans. Signal Processing*, vol. 55, pp. 5782–5795, Dec. 2007.

[16] L. Tong, B. M. Sadler, and M. Dong, "Pilot-assisted wireless transmissions," *IEEE Signal Processing Mag.*, vol. 21, pp. 12–25, Nov. 2004.

[17] A. P. Kannu and P. Schniter, "Design and analysis of MMSE pilot-aided cyclic-prefixed block transmissions for doubly selective channels," *IEEE Trans. Signal Processing*, vol. 56, pp. 1148–1160, Mar. 2008.

[18] A. P. Kannu and P. Schniter, "On the spectral efficiency of noncoherent doubly selective block-fading channels," *IEEE Trans. Inform. Theory*. Submitted.

[19] M. Nissilä and S. Pasupathy, "Adaptive Bayesian and EM-based detectors for frequency-selective fading channels," *IEEE Trans. Commun.*, vol. 51, pp. 1325–1336, Aug. 2003.

[20] S.-J. Hwang and P. Schniter, "Fast noncoherent decoding of block transmissions over doubly dispersive channels," in *Proc. Asilomar Conf. Signals, Systems and Computers*, Nov. 2007.

[21] M. K. Tsatsanis and G. B. Giannakis, "Modeling and equalization of rapidly fading channels," *Int. J. Adaptive Control & Signal Processing*, vol. 10, pp. 159–176, Mar. 1996.

[22] T. H. Eggen, A. B. Baggeroer, and J. C. Preisig, "Communication over Doppler spread channels—Part I: Channel and receiver presentation," *IEEE J. Oceanic Eng.*, vol. 25, pp. 62–71, Jan. 2000.

[23] W. Li and J. C. Preisig, "Estimation and equalization of rapidly varying sparse acoustic communication channels," in *Proc. IEEE OCEANS*, Sept. 2006.

[24] S.-J. Hwang and P. Schniter, "Efficient communication over highly spread underwater acoustic channels," in *Proc. ACM Int. Workshop Underwater Networks (WUWNet)*, Sept. 2007.

[25] B. M. Hochwald and S. ten Brink, "Achieving near-capacity on a multiple-antenna channel," *IEEE Trans. Commun.*, vol. 51, pp. 389–399, Mar. 2003.

[26] Y. L. C. de Jong and T. J. Willink, "Iterative tree search detection for MIMO wireless systems," *IEEE Trans. Commun.*, vol. 53, pp. 930–935, June 2005.

[27] J. B. Anderson and S. Mohan, "Sequential decoding algorithms: A survey and cost analysis," *IEEE Trans. Commun.*, vol. 32, pp. 169–172, 1984.

[28] B. D. Hart, "Maximum likelihood sequence detection using a pilot tone," *IEEE Trans. Veh. Technol.*, vol. 49, pp. 550–560, Mar. 2000.

[29] I. Kozintsev, "Matlab programs for encoding and decoding of LDPC codes over GF(2^m)." http://www.kozintsev.net/soft.html.

[30] Z. Tang, R. C. Cannizzaro, G. Leus, and P. Banelli, "Pilot-assisted time-varying channel estimation for OFDM systems," *IEEE Trans. Signal Processing*, vol. 55, pp. 2226–2238, May 2007.

[31] W. C. Jakes, *Microwave Mobile Communications*. Wiley, 1974. [reprinted by IEEE Press].

Sung-Jun Hwang received the B.S. and M.S. degrees in electronic engineering from Yonsei University, Seoul, Korea, in 1993 and 1995, respectively. He worked as an engineer for Samsung Electronics, Co. Ltd., in Seoul, Korea, from 1995 to 2000, and Samsung Thales, Co. Ltd., in Kiheung, Korea, from 2000 to 2003.

Since 2004 he has been working toward the Ph.D. degree in electrical and computer engineering at The Ohio State University, Columbus, OH. His primary research interest is noncoherent communication over time and frequency selective channels.

Philip Schniter received the B.S. and M.S. degrees in Electrical and Computer Engineering from the University of Illinois at Urbana-Champaign in 1992 and 1993, respectively. From 1993 to 1996 he was employed by Tektronix Inc. in Beaverton, OR as a systems engineer. In 2000, he received the Ph.D. degree in Electrical Engineering from Cornell University in Ithaca, NY. Subsequently, he joined the Department of Electrical and Computer Engineering at The Ohio State University in Columbus, OH, where he is now an Associate Professor. He currently serves as an Associate Editor for IEEE Signal Processing Letters and sits on the IEEE Signal Processing for Communications Technical Committee.

While pursuing his Ph.D. degree, Dr. Schniter received a Schlumberger Fellowship and an Intel Foundation Fellowship. He was awarded the 1999 Prize Paper Award from the IEEE Energy Development and Power Generation Committee for work relating to his M.S. thesis. In 2003, he received the National Science Foundation CAREER Award, and, in 2005, the OSU College of Engineering Lumley Research Award.

Dr. Schniter's areas of research include signal processing and communication theory.